JOURNAL OF MATERIALS SCIENCE 30 (1995) 923–931

Roles of alumina in zirconia-based solid electrolyte

XIN GUO*, RUNZHANG YUAN
State Key Laboratory for Synthesis and Processing of Advanced Materials, Wuhan University of Technology, Wuhan, Hubei Province 430070, People's Republic of China

Up to 5 mol% Al_2O_3 was added to 9 mol% Y_2O_3-stabilized ZrO_2, and the roles of Al_2O_3 were systematically studied by means of the complex impedance approach, the positron annihilation technique, SEM, TEM, and electron probe microanalysis from the following aspects: (1) the existence of forms of Al_2O_3 in ZrO_2, (2) the effects of Al_2O_3 on the microstructure of ZrO_2, (3) the effects of Al_2O_3 on the resistance of ZrO_2, (4) the microstructure and property changes of ZrO_2 with Al_2O_3 addition during ageing at 940 °C. Two types of grain boundary phase, crystal and amorphous, were discovered. The Al_2O_3 segregation at grain boundaries can promote the mobility of the grain boundaries and thus results in a low density, because of entrapped pores. The Al_2O_3 addition decreases the grain-boundary resistance in two ways: to scavenge the SiO_2 and CaO located at grain boundaries, and to form crystal grain-boundary phases with very high crystal defect concentrations. Ordered microdomains of $Zr_3Y_4O_{12}$ were precipitated from ZrO_2 grains during ageing, and aluminium was found to facilitate the precipitation.

1. Introduction

Cubic ZrO_2 has good oxygen ion conductivity at temperatures above 600 °C, and has been widely used in oxygen sensors and fuel cells as a solid electrolyte [1]. In these applications, a certain mechanical strength and impermeability are often required of the ZrO_2-based solid electrolyte. In order to enhance the densification of ZrO_2 during sintering, a certain amount of Al_2O_3 is added to ZrO_2 [2]. After further studies, it was discovered that Al_2O_3 can also decrease the resistance of ZrO_2. Miyayama *et al.* [3] have studied 8 mol % Y_2O_3-stabilized ZrO_2 with the addition of 0–1.0 mol % Al_2O_3, and found that the ZrO_2 resistance increases with increasing Al_2O_3 concentration up to 0.6 mol %, but decreases when the Al_2O_3 concentration was > 0.6 mol%. Much research has been done on the roles of Al_2O_3 in ZrO_2, but results are often contradictory [4–6]. In the present work, the Al_2O_3 addition was increased up to 5 mol%, and the roles of Al_2O_3 in the ZrO_2-based solid electrolyte were systematically studied from the following aspects: (1) the forms of Al_2O_3 existing in ZrO_2, (2) the effects of Al_2O_3 on the microstructure of ZrO_2, (3) the effects of Al_2O_3 on the resistance of ZrO_2, and (4) the microstructure and property changes of ZrO_2 with Al_2O_3 addition during ageing.

2. Experimental procedure

2.1. Preparation of specimens

The compositions of specimens are listed in Table I. Powders used to produce the specimens were prepared from $ZrOCl_2 \cdot 8H_2O$, YCl_3 and $AlCl_3$ by a co-precipitation method, and the average particle sizes as measured by a centrifugal particle size analyser (type SA-CP3) were 0.45, 0.40 and 0.48 μm, respectively. The powders were subsequently pressed into pellets (22 mm diameter, 4 mm thick) at 200 MPa, then sintered at 1520, 1540, 1580, and 1600 °C for 2 h. Platinum electrodes were applied to the ZrO_2 specimens by the decomposition of chloroplatinic acid at 1000 °C.

2.2. Measurement and analyses

The specimens were subjected to the following measurements and analyses. (1) Bulk densities were recorded by buoyancy measurements. (2) Average grain-size measurements were obtained from the scanning electron micrographs of the surfaces of as-sintered specimens, and calculation of the grain size was based on a method described by Fullman [7]. (3) Resistances were measured by the complex impedance approach in the frequency range 20 Hz–1 MHz with a HP4285A precision LCR meter, and the grain-boundary resistances were separated out by analysis of the

TABLE I Composition of specimens

Specimen	Composition
0AYZ	ZrO_2–9 mol % Y_2O_3
1.5AYZ	ZrO_2–9 mol % Y_2O_3– 1.5 mol % Al_2O_3
5AYZ	ZrO_2–9 mol % Y_2O_3–5 mol % Al_2O_3

* Author to whom all correspondence should be addressed.

0022–2461

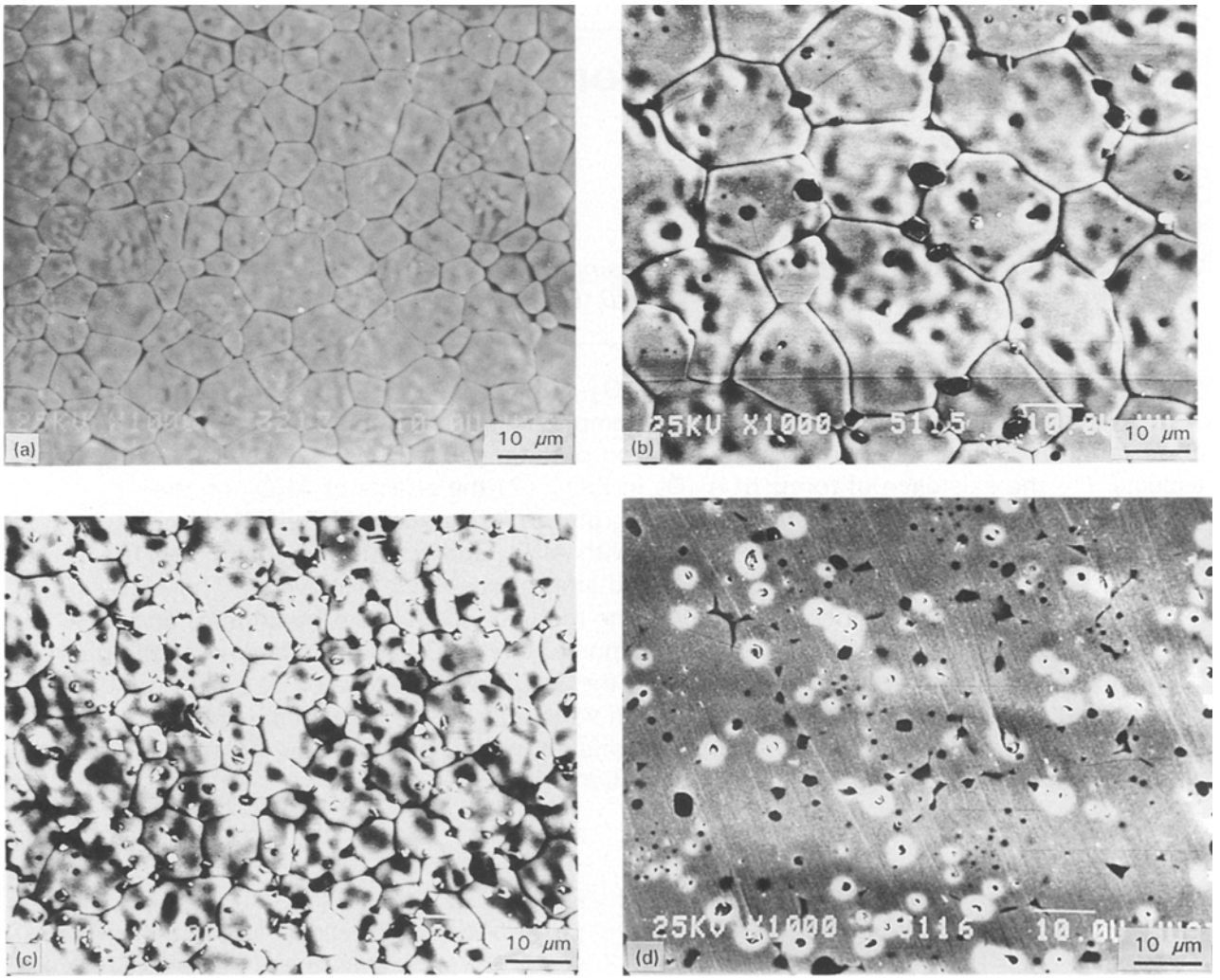

Figure 1 Scanning electron micrographs of the surfaces of as-sintered specimens. (a) OAYZ, (b) 1.5AYZ, (c) 5AYZ, (d) 1.5AYZ, polished surface.

complex plots. (4) Aluminium distribution information inside the specimens was examined by electron probe microanalysis (EPMA, type JCXA-733) on the specimens polished and coated with carbon. (5) Microstructure studies were carried out by SEM (type JSM-35C) and TEM (type H-800, Philips-CM12/STEM). (6) Crystal defect changes were detected by the positron annihilation technique (Canberra Series 35).

3. Results and discussion

3.1. Forms of Al_2O_3 in ZrO_2

The solubility of Al_2O_3 in ZrO_2 grains is very low; only 0.5 mol % Al_2O_3 can be dissolved in Y_2O_3-stabilized ZrO_2 sintered at 1700 °C and cooled at 220 °C h^{-1} [3], and the solubility of Al_2O_3 is about 0.1 mol % when sintered at 1300 °C [5]. It is thus obvious that the Al_2O_3 additions in this work are far beyond the Al_2O_3 solubility.

3.1.1. SEM

Fig. 1 shows scanning electron micrographs of the surfaces of the as-sintered specimens 0AYZ, 1.5AYZ, and 5AYZ, and the polished surface of the specimen 1.5AYZ. The specimen 0AYZ has a homogeneous monophase structure, while Al_2O_3 particles can be observed as bright or dark spots in specimens 1.5AYZ and 5AYZ; the Al_2O_3 particles are situated both inter- and intragranularly. Because there are quite large differences in the elastic modulus and the thermal expansion coefficient between Al_2O_3 and ZrO_2, the intragranular Al_2O_3 partilces are always accompanied by pores, which can be seen from the polished surface.

3.1.2. EPMA

Fig. 2 shows the EPMA analysis results; (a) and (c) are scattered electron images, and (b) and (d) show the aluminium distributions. From these photographs, it can be seen that aluminium is mainly segregated at grain boundaries, and the aluminium segregation is more serious in specimen 5AYZ. Some small dark spots inside the grains shown in the scattered electron images are Al_2O_3 particles and pores. No apparent enrichment of silicon or calcium at grain boundaries was observed.

3.1.3. TEM

Because of the segregation of Al_2O_3 and impurities at grain boundaries, grain-boundary phases were often formed. Two types of grain-boundary phase were

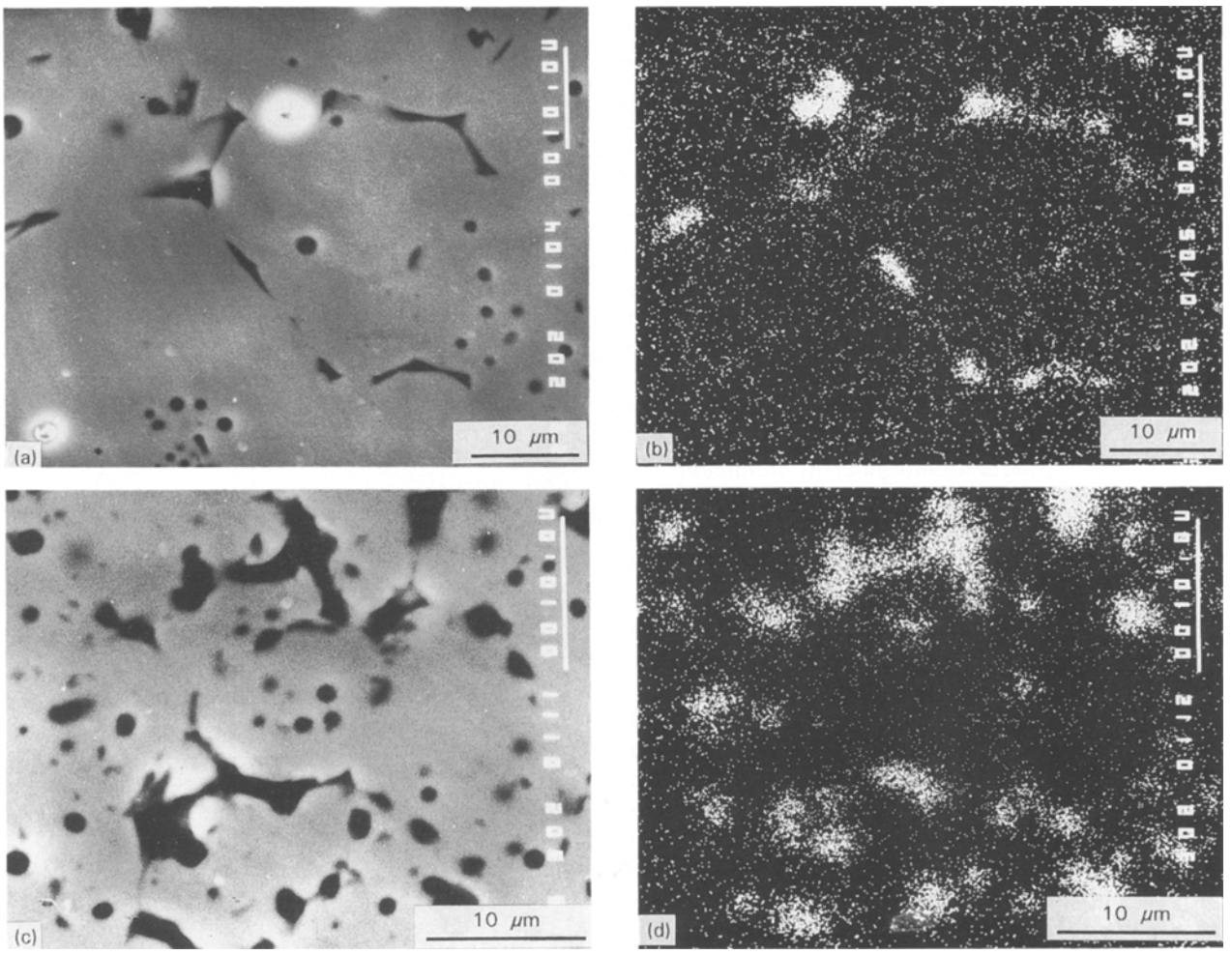

Figure 2 EPMA photographs of specimens with different Al_2O_3 content. (a, b) 1.5AYZ, (c, d) 5AYZ.

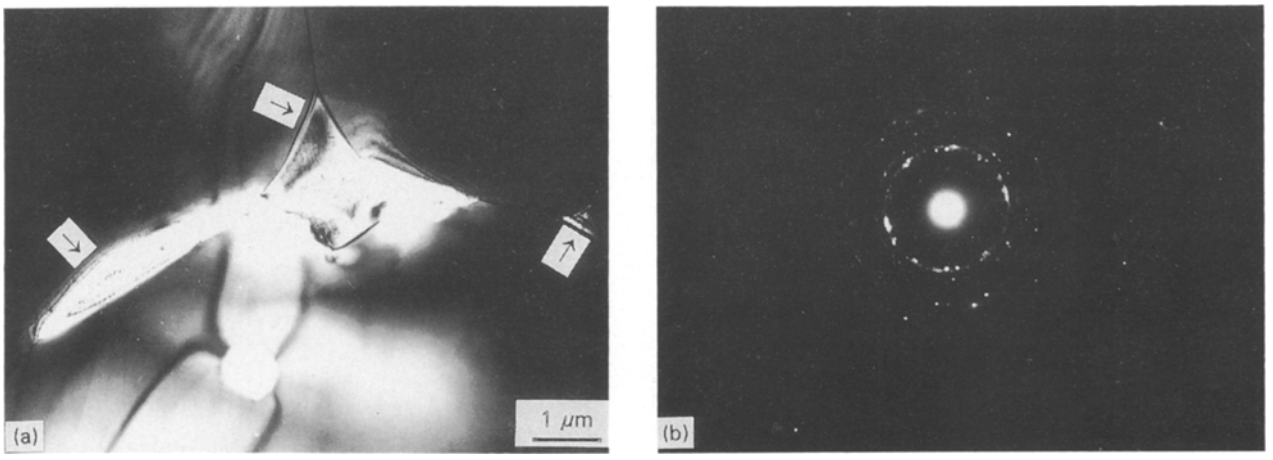

Figure 3 Transmission electron micrograph of crystal grain-boundary phases. (a) Bright-field image, (b) SADP. The arrows indicate the grain-boundary phases.

discovered in specimens with Al_2O_3 addition, one type is shown in Fig. 3. The small bright particle situated at the triple point of ZrO_2 grains is an Al_2O_3 particle (Fig. 3a); the grain-boundary phases have a peculiar morphology. Fig. 3b is the SADP of the grain-boundary phases; the diffraction rings indicate that the grain-boundary phases consist of large amounts of crystallites. The ratio of the square radii of the diffraction rings are

$$R_1^2 : R_2^2 : R_3^2 : R_4^2 : R_5^2 : R_6^2 \approx 1 : 2 : 3 : 6 : 7 : 9 \quad (1)$$

According to the ratio and brightness distribution of the diffraction rings, these crystallites do not have the crystal structure of α-Al_2O_3 nor cubic ZrO_2; because of the large errors usually involved in electron diffractions, it is still difficult to determine the crystal

TABLE II Composition of crystal grain-boundary phases measured by EDAX

Element	wt %	at %
Al	2.62	8.29
Y	15.76	15.17
Zr	81.62	76.54

structure of the crystallites. The composition of the grain-boundary phases measured by EDAX is given in Table II; enrichment of aluminium was found, and no impurities such as silicon or calcium were detected. However, for the crystal grain-boundary phases in different regions of the specimen, different SADP patterns were produced and different aluminium, yttrium and zirconium concentrations are measured by EDAX. The phases may be concluded to be a kind of aluminium-rich compound with a chemical formula $(Al_2O_3)_x(Y_2O_3)_y(ZrO_2)_z$ $(x + y + z = 1)$. The number of crystal grain-boundary phases is quite large; they are distributed at grain boundaries and Al_2O_3/ZrO_2 interfaces.

Another type of grain-boundary phase is shown in Fig. 4, this type of grain-boundary phase is rarely found in the specimens, they are distributed at triple points (Fig. 4a) and Al_2O_3/ZrO_2 interfaces (Fig. 4b). The SADP of the grain-boundary phases (Fig. 4c) indicates that they are amorphous, and corresponding EDAX measurement (Table III) reveals impurities silicon and calcium, besides the enrichment of aluminium. The grain boundaries without amorphous phases are quite clean; no impurities such as silicon and calcium are present there.

According to the above analyses, we can conclude that three forms of Al_2O_3 in ZrO_2, exist; they are: (1) a very small amount of Al_2O_3 dissolved in ZrO_2 grains, (2) the surplus Al_2O_3 then forms Al_2O_3 particles, which are extensively situated inter- and intragranularly, and (3) Al_2O_3 segregates at grain boundaries, and forms the crystals and the amorphous aluminium-rich grain-boundary phases, the amorphous one containing impurities such as silicon and calcium.

3.2. Effects of Al_2O_3 on the microstructure of ZrO_2

It is generally accepted that Al_2O_3 can enhance the densification of ZrO_2. According to Radford and Bratton [2], Al_2O_3 formed liquid phase at grain boundaries, but Bernard [5] found no evidence for liquid-phase formation during sintering at 1300 °C;

TABLE III Composition of amorphous grain-boundary phases measured by EDAX

Element	wt %	Oxide (%)
Al	9.26	17.50
Si	29.40	62.91
Ca	8.00	11.20
Y	4.43	5.63
Zr	2.48	3.35

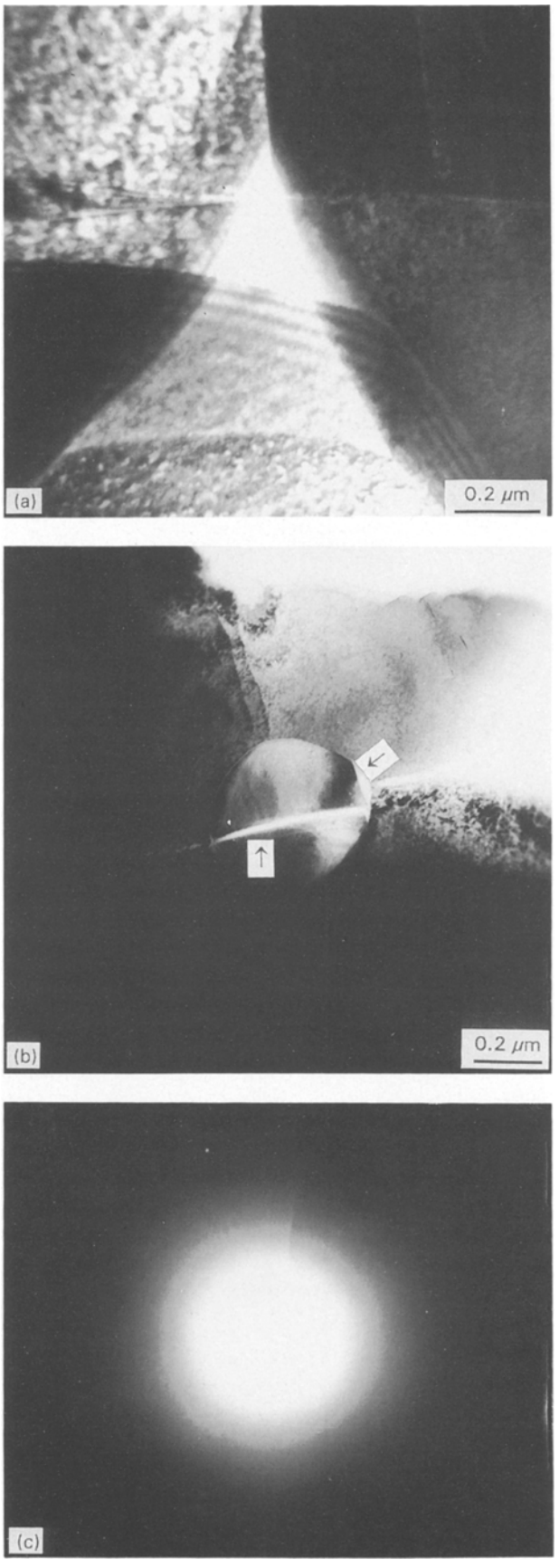

Figure 4 Transmission electron micrographs of amorphous grain-boundary phases. (a, b) Bright-field image, (c) SADP. The arrows indicate the grain-boundary phases.

the added Al_2O_3 was present principally as second-phase particles, which pin grain boundaries, and a fine grain size and densified microstructure resulted. However, the results in this work prove that Al_2O_3

improves the mobility of grain boundaries, and that the fast-moving grain boundaries entrap pores in grains resulting in low densities.

3.2.1. Bulk density

The bulk densities of the specimens sintered at various temperatures are shown in Fig. 5. Specimen 0AYZ attains high density when sintered at 1540 °C, but specimen 1.5AYZ can only attain an equivalent density when sintered at 1600 °C. The densities of specimen 5AYZ are relatively low, indicating that Al_2O_3 lowers the sintering density of ZrO_2 and the effect of Al_2O_3 is more serious with increasing Al_2O_3 content.

3.2.2. Average grain size

The average grain-size measurement results are plotted in Fig. 6. Three features can be seen from Fig. 6: (1) specimen 0AYZ always has the smallest average grain size, notwithstanding sintering temperatures; (2) the average grain size of specimen 1.5AYZ increases dramatically with increasing sintering temperature, (3) specimen 5AYZ has large average grain size when sintered at low temperature, and the grains grow very slowly when the sintering temperature is increased. This fact indicates that Al_2O_3 can promote grain growth.

3.2.3. Discussion

In the ZrO_2 system, the control step of densification is the bulk diffusion of Zr^{4+} which is affected by the defect structure of ZrO_2 [8, 9]. However, the defect structure of ZrO_2 is essentially controlled by dopant, because the dopant is dissolved in ZrO_2 in large amounts [9]. The solubility of Al_2O_3 in ZrO_2 is very small, so the effect of Al_2O_3 on the defect structure is negligible, thus Al_2O_3 has virtually no effect on the densification of ZrO_2, so the reason why the specimens with Al_2O_3 additions have lower densities may be that ZrO_2 grains grow too fast. In the ZrO_2 system, the grain-growth mechanism is surface diffusion [8, 9].

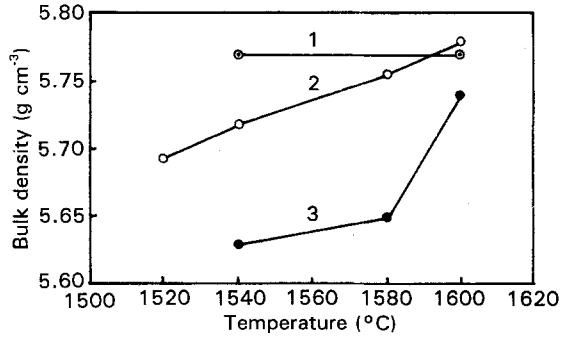

Figure 5 Bulk densities of specimens sintered at various temperatures. 1, OAYZ; 2, 1.5AYZ; 3, 5AYZ.

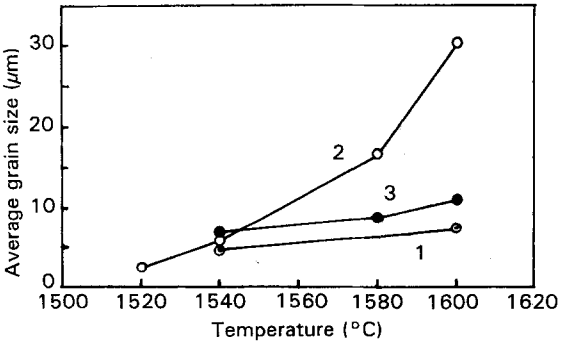

Figure 6 Average grain sizes of specimens sintered at various temperatures. 1, OAYZ; 2, 1.5AYZ; 3, 5AYZ.

The Al_2O_3 addition has a dual effect on grain growth. First, the intergranular Al_2O_3 particles pin grain boundaries, which can be seen from the fact that the grains of specimen 5AYZ grow slowly with increasing sintering temperature, and the fact that specimen 5AYZ has a much smaller grain size than specimen, 1.5AYZ when sintered at 1600 °C. Because of the pinning of the grain boundaries by the intergranular Al_2O_3 particles, specimen 5AYZ can eliminate more pores, so the density is greatly increased after sintering at 1600 °C.

Second, the Al_2O_3 segregated at grain boundaries can improve the mobility of the boundaries. This is explained below. The velocity of a grain boundary without any pores is

$$V_b = F_b M_b \tag{2}$$

where F_b is the grain-boundary movement driving force which is determined by the curvature of the grain boundary [10]

$$F_b = \frac{2\gamma_b \Omega}{\omega R} \tag{3}$$

where M_b is the mobility of the grain boundary, which is given by

$$M_b = \frac{D}{kT} \tag{4}$$

γ_b is the grain-boundary energy, Ω is the atomic volume, ω is the grain-boundary thickness, R is the curvature of the grain boundary, D is the grain-boundary diffusion coefficient, and k is Boltzmann's constant. Then the grain-boundary velocity is

$$V_b = \frac{2D\gamma_b \Omega}{kT\omega R} \tag{5}$$

The Al_2O_3 segregation at grain boundaries may increase the grain-boundary diffusion coefficient, D, thus V_b is increased. The above experimental results demonstrate that the sum of these two effects of Al_2O_3 is to promote the grain growth.

Pores should be eliminated as much as possible in order to obtain a densified microstructure. Alexander and Baluffi [11] were the first to observe that pores entrapped inside grains are remarkably stable, and that the only pores to disappear are those intersected by grain boundaries. The mobility of a pore is given by [12]

$$M_p = \frac{D_s \delta \Omega}{kT\pi r^4} \tag{6}$$

where D_s is the surface diffusion coefficient, δ is the thickness of surface diffusion layer, r is the radius of the pore. Like the grain-boundary diffusion coefficient, D, D_s may also be increased because of the Al_2O_3 segregation, thus pore movement is also accelerated. When the rapid movement of grain boundaries does not match that of pores, the pores are entrapped inside grains; this is the reason why the specimens with Al_2O_3 addition have lower densities. The rapidly moving grain boundaries can also overcome the pinning of Al_2O_3 particles and entrap them inside grains, this phenomenon is clearly shown in Fig. 1.

3.3. Effect of Al_2O_3 on the resistance of ZrO_2

Al_2O_3 can decrease ZrO_2 resistance; Butler and Drennan [13] suggested that this is because Al_2O_3 acts as a scavenger for SiO_2 located at grain boundaries and $Al_6Si_2O_{13}$ is formed. In the present work, the effects of Al_2O_3 are reanalysed from the aspects of microstructure and crystal defects, and a new mechanism is proposed to explain the effects of Al_2O_3. The specimens used were all sintered at 1600 °C.

3.3.1. Resistance

The complex impedance approach has been used extensively in the examination and development of solid electrolyte after the initial report by Bauerle [14]. This approach can effectively probe the grain resistance as well as the resistance across grain boundaries and electrode/electrolyte interface.

The resistances of the specimens were measured at 440 and 500 °C; the results are listed in Table IV. The grain resistance of specimen 0AYZ is smaller than those of specimens 1.5AYZ and 5AYZ, whereas the grain-boundary resistance of specimen 0AYZ is much higher than those of specimens 1.5AYZ and 5AYZ; specimen 5AYZ has the smallest grain-boundary resistance.

Activation energies for grain and grain-boundary resistance can be calculated from the Arrhenius equation

$$R = A\exp(E/kT) \tag{7}$$

where k and T have their usual meanings. The values are also listed in Table IV. Specimen 0AYZ has the smallest grain-resistance activation energy, E_g, but the largest grain-boundary resistance activation energy E_{gb}, and E_{gb} decreases with increasing Al_2O_3 content.

TABLE IV Resistances and activation energies of the specimens

Specimen	Measured at 440 °C		Measured at 500 °C		Activation energy (KJ mol^{-1})	
	R_g (Ω)	R_{gb} (Ω)	R_g (Ω)	R_{gb} (Ω)	E_g	E_{gb}
0AYZ	200	1400	100	300	52.9	117.6
1.5AYZ	700	215	195	50	97.5	111.3
5AYZ	600	175	175	50	94.0	95.6

3.3.2. Positron annihilation

The measurements of positron lifetime spectra were carried out at room temperature, 21 ± 1 °C, by a fast–fast coincidence lifetime spectrometer with a resolution of 230 ps. A ^{22}NaCl positron source was used in the measurements. The normal specimen–source–specimen sandwich arrangement was adopted. A total of 10^6 counts in each spectrum was collected. After substraction of the source and background contribution, all lifetime spectra were analysed with three components by the program POSITRONFIT EXTENDED. Lifetimes τ_1, τ_2 and τ_3 and their relative intensities I_1, I_2 and I_3, were obtained (Table V). The long lifetime component τ_3, whose intensity is about 1.4%, arises from the annihilation in the positron source and associated foils, and/or interfaces that are unavoidable with the sandwich arrangement, so τ_3 can be neglected. The short lifetime component, τ_1, reflects the positron annihilation feature of perfect crystal, and τ_2 is the positron lifetime in crystal defects. According to the two-state trapping model [15], we can derive the positron annihilation rate K

$$K = I_2 \Big/ \left(\frac{1}{\tau_1} - \frac{1}{\tau_2}\right) \tag{8}$$

The K values are listed in Table V. K can also be expressed as $K = \mu c$, where c is the concentration of defects, μ is considered to be constant when the type or the structure of defects do not change, thus the change of K can roughly reflect the change of defect concentration. K increases when Al_2O_3 is added to ZrO_2; this tendency is opposite to that of the grain-boundary resistance, in other words, with increasing Al_2O_3 content, the defect concentrations of the specimens are increased, and consequently the resistances are decreased.

3.3.3. Discussion

As shown in Table IV, Al_2O_3 increases the grain resistance; this is because the interagranular Al_2O_3 particles and the accompanying pores are insulating, and they are obstacles to the migration of oxygen ions. This also explains why specimen 0AYZ has the smallest grain-resistance activation energy.

There are two types of grain-boundary phase in ZrO_2, crystal and amorphous. Table IV shows that Al_2O_3 decreases the grain-boundary resistance, this phenomenon may be explained by two mechanisms that are related to the two types of grain-boundary phase.

Mechanism I: the Al_2O_3 addition scavenges SiO_2 located at grain boundaries and results in a low grain-boundary resistance; this is similar to Butler and

TABLE V Positron lifetime parameters

Specimen	τ_1 (ps)	τ_2 (ps)	τ_3 (ps)	I_1 (%)	I_2 (%)	I_3 (%)	K (μ s^{-1})
0AYZ	239	269	1802	90.5	8.2	1.3	38.3
1.5AYZ	205	353	1685	90.9	7.6	1.5	155.4
5AYZ	204	374	1806	92.0	6.9	1.2	153.7

Drennan's result [13]. The only difference from Butler and Drennan's experiment is that the specimens used in this paper contain CaO in addition to SiO_2, according to the $CaO–Al_2O_3–SiO_2$ phase diagram [16], CaO, Al_2O_3 and SiO_2, with the concentration relation listed in Table III, will react with each other according to the following equation

$$CaO + Al_2O_3 + 2SiO_2 \rightarrow CaAl_2Si_2O_8 \quad (9)$$

The impurities CaO, SiO_2 are transported by grain-boundary diffusion to the triple points with high Al_2O_3 concentration and the Al_2O_3 particle surfaces, and by the above chemical reaction, the grain-boundary impurities are scavenged; as a result, E_{gb} is decreased.

Mechanism II: The crystal grain-boundary phases contain no CaO or SiO_2 so mechanism I cannot explain all the experimental phenomena. In addition, the positron annihilation results show that Al_2O_3 increases the crystal-defect concentration in ZrO_2. The defect can be roughly divided into two main parts: the defects in grains and those in the crystal grain-boundary phases. The defects in grains are determined by the dopant Y_2O_3, and the Al_2O_3 solubility in grains is very low, so the effect of Al_2O_3 on the grain defects is negligible, indicating that the increased crystal-defect concentration is a result of the increasing of crystal defects in the crystal grain-boundary phases, and consequently the resistance of the crystal grain-boundary phases is very low, so the grain-boundary resistance is subsequently decreased. Thus a new mechanism is derived as follows: Al_2O_3 segregates at grain boundaries, and forms crystal grain-boundary phases with very high defect concentration, so the grain-boundary resistance is decreased.

3.4. Microstructure and property changes of the ZrO_2 with Al_2O_3 addition during ageing

ZrO_2-based solid electrolyte used in oxygen sensors or fuel cells must endure elevated temperature; this is somewhat like a high-temperature ageing process. High-temperature ageing can cause an increased ZrO_2 resistance. Baukal has studied the ageing of Y_2O_3-stabilized ZrO_2[17], Hudson and Moseley investigated the ageing of CaO-stabilized ZrO_2 [18], they all agreed that the increased resistance is due to an order–disorder transformation in grains, microdomains of $Zr_3Y_4O_{12}$ or $CaZrO_9$ are precipitated, as sometimes is monoclinic ZrO_2. We examined the ageing feature of the ZrO_2 with Al_2O_3 addition, and discusses the effect of Al_2O_3. In experiments, specimens sintered at 1580 °C were used, and they were aged at 940 °C for up to 222 h. After ageing, the resistance and microstructure of the specimens were examined. The transformations of the grain-boundary phases during ageing are very complicated; when examining different specimens aged for the same period, different results are often obtained. For the sake of simplicity, we only deal with the changes in grains.

3.4.1. Resistance

The grain resistances of specimen 1.5AYZ measured at 500 °C are plotted against ageing time in Fig. 7. The grain resistance is gradually increased at the ageing stage of 0–48 h, and then remains principally constant.

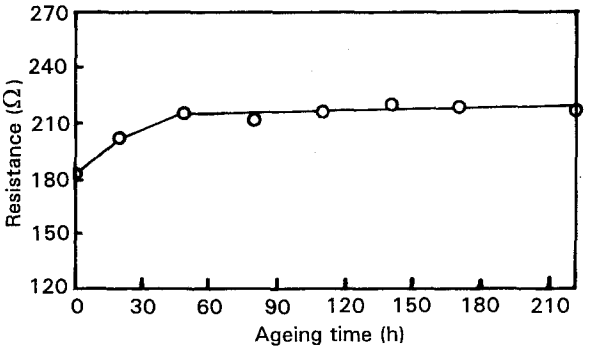

Figure 7 Change of grain resistance of the specimen 1.5AYZ during ageing.

3.4.2. TEM

Fig. 8 shows the morphologies of the precipitates of specimen 1.5AYZ aged for 222 h and the corresponding SADPs. It can be seen from Fig. 8a that much fine dark phase is precipitated from the grain, the diffraction pattern in Fig. 8b contains three distinct groups, ZrO_2 matrix diffraction spots $[\bar{1}\,1\,3]_0$, ZrO_2 matrix high-level Laue spots $[\bar{1}\,1\,3]_{+1}$, and superstructure spots. The superstructure spots are reflected from the dark precipitates, demonstrating that the precipitates are ordered microdomains; according to the SADP, the orientation relation between the microdomains and the matrix is

$$[\bar{1}\,1\,3]_{Zro_2} \parallel [\bar{1}\,1\,3]_p \quad (10)$$

$$(\bar{4}\,2\,\bar{2})_{Zro_2} \parallel (\bar{2}\,1\,\bar{1})_p \quad (11)$$

Fig. 8d shows another kind of precipitate in the same specimen. Compared with that shown in Fig. 8a, the precipitates are quite large in size and in quantity; the corresponding SADP (Fig. 8e) is a diffraction ring pattern, indicating that the precipitates have lost the orientation relation with the matrix. The ratio of the square radii of the diffraction rings is

$$R_1^2 : R_2^2 : R_3^2 : R_4^2 ; R_5^2 \approx 3 : 4 : 8 : 11 : 12 \quad (12)$$

thus the precipitates have fcc structure. After calculating the crystal-plane distances from the SADPs shown in Fig. 8b and e and consulting the JCPDS files, the precipitates are judged to be $Zr_3Y_4O_{12}$. Fig. 7 indicates that the precipitation of $Zr_3Y_4O_{12}$ increases the grain resistance, and from the grain-resistance changing process, it can be inferred that the microdomains $Zr_3Y_4O_{12}$ are precipitated at the ageing stage of 0–48 h. No monoclinic ZrO_2 precipitates were discovered in the specimen. The composition of the region shown in Fig. 8d was measured by EDAX; a certain amount of aluminium and silicon was detected (see Table VI).

Fig. 9 shows the precipitates in the specimen 5AYZ and the corresponding SADP. The precipitates in the specimen 5AYZ are also large in size and quantity;

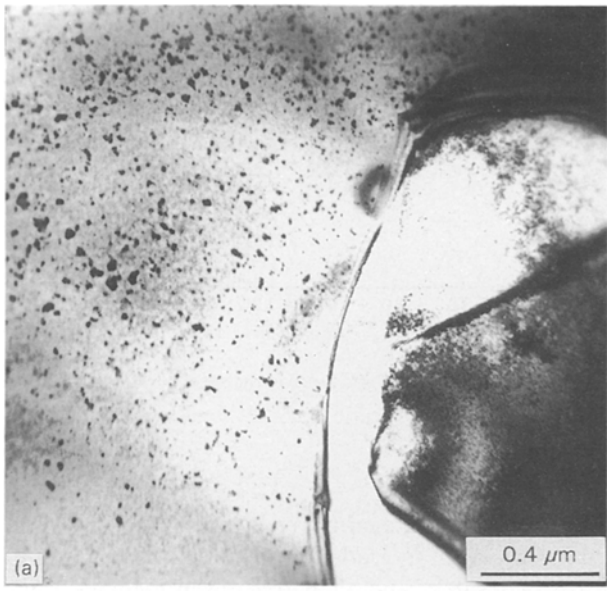

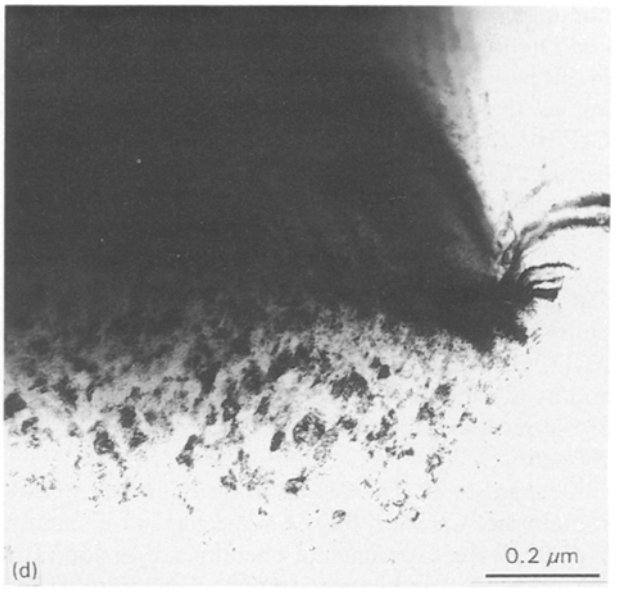

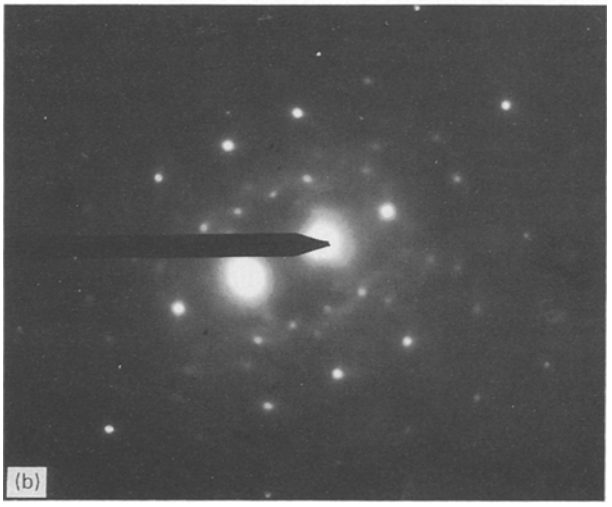

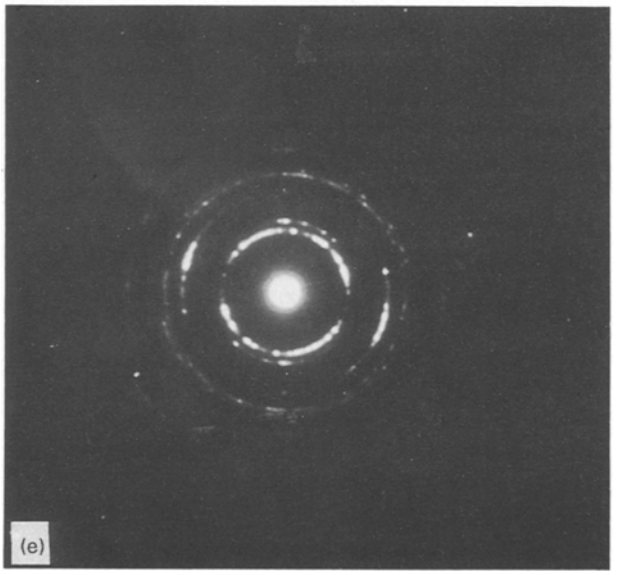

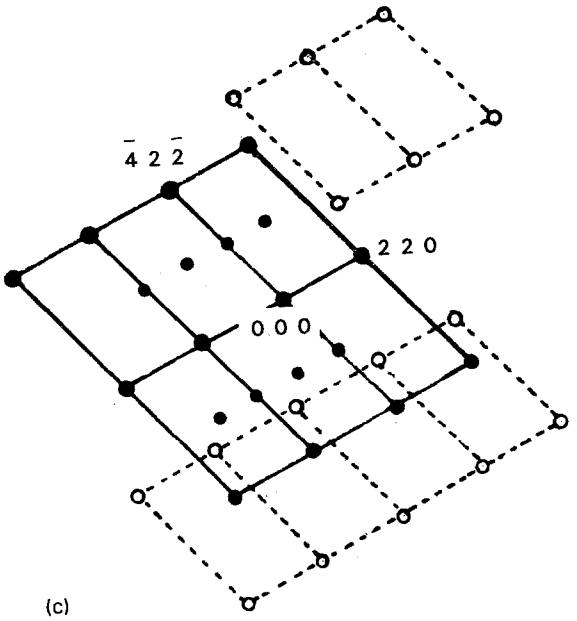

Figure 8 Transmission electron micrographs of precipitates in the grain of specimen 1.5AYZ. (a, d) Bright-field images; (b, c, e) SADP.

they have no orientation relation with the matrix. No such precipitate as that shown in Fig. 8a was discovered in specimen 5AYZ. The precipitates shown in Fig. 9a and that shown in Fig. 8d have two features in common: (1) they are all quite large in size and quantity, (2) they all have no orientation relation with the matrix; so it can be concluded that aluminium can facilitate the precipitation and growth of $Zr_3Y_4O_{12}$.

4. Conclusions

1. The solubility of Al_2O_3 in ZrO_2 is very low; part of the surplus Al_2O_3 forms Al_2O_3 particles, another part segregates at grain boundaries and forms aluminium-rich grain-boundary phases. There are two types of grain boundary phase, i.e., crystal and amorphous; the amorphous one contains impurities of silicon and calcium.

TABLE VI Composition of the region shown in Fig. 8d measured by EDAX

Element	wt %	Oxide (%)
Al	7.04	13.30
Si	11.05	23.64
Y	9.13	11.60
Zr	38.59	52.13

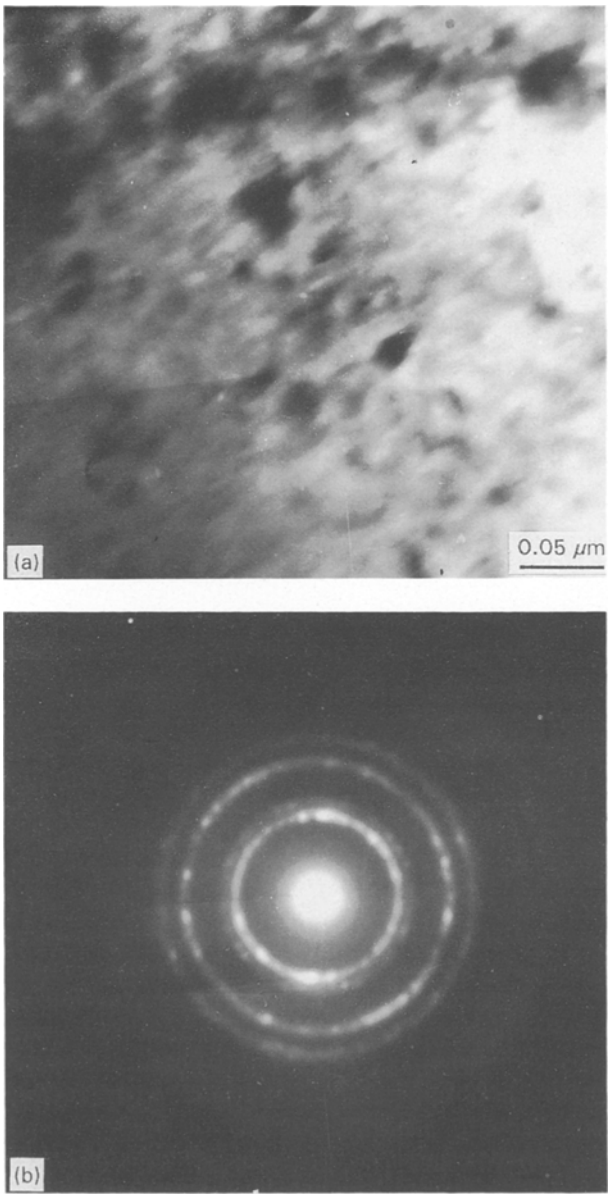

Figure 9 Transmission electron micrographs of precipitates in the grain of specimen 5AYZ. (a) Bright-field image, (b) SADP.

2. Al_2O_3 can remarkably promote the growth of ZrO_2 grains; the pores are entrapped inside the grains, resulting in a low density.

3. Al_2O_3 lowers the ZrO_2 grain-boundary resistance in two ways: (i) Al_2O_3 reacts with SiO_2 and CaO to scavenge the impurities from grain boundaries, and (ii) Al_2O_3 segregated at grain boundaries forms crystal phases with a very high defect concentration.

4. The precipitation of $Zr_3Y_4O_{12}$ from ZrO_2 grains increases the grain resistance during ageing, and aluminium facilitates the precipitation.

References

1. R. STEVENS, "Zirconia and Zirconia Ceramics," 2nd Edn (Magnesium Elektron, 1986) p. 38.
2. K. C. RADFORD and R. J. BRATTON, *J. Mater. Sci.* **14** (1979) 59.
3. M. MIYAYAMA, H. YANAGIDA and A. ASADA, *Am. Ceram. Soc. Bull.* **64** (1986) 660.
4. N. M. BEEKMANS and L. HEYNE, *Electrochim. Acta* **21** (1976) 303.
5. H. BERNARD, Rep. CEA-R-5090, Commissariat à l'Energie Atomique, CEN-Saclay, France, (1981) p. 117.
6. M. J. VERKERK, A. J. A. WINNUBST and A. J. BURGGRAAF, *J. Mater. Sci.* **17** (1982) 3113.
7. R. L. FULLMAN, *J. Metals AIME Trans.* **5** (1953) 447.
8. P. J. JORGENSEN, in "Sintering and Related Phenomena", edited by G. C. Kuczynski, N. A. Hooton and C. F. Gibbon (Gordon Breach, New York, 1967) p. 401.
9. S. WU and R. J. BROOK, *Solid State Ionics* **14** (1984) 123.
10. R. J. BROOK, in "Treatise on Materials Science and Technology", Vol. 9, edited by F. F. Wang (Academic Press, New York, 1976) p. 331.
11. B. H. ALEXANDER and R. W. BALUFFI, *Acta Metall.* **5** (1957) 666.
12. P. G. SHEWMON, *Trans. AIME* **230** (1964) 1134.
13. E. P. BUTLER and J. DRENNAN, *J. Am. Ceram. Soc.* **65** (1982) 474.
14. J. E. BAUERLE, *J. Phys. Chem. Solids* **30** (1969) 2657.
15. W. BRANDT and A. DUPASQUIER, "Positron Solid State Physics", (North-Holland, Amsterdam, 1983) pp. 24, 200.
16. G. GOTTWALD, K. FORKEL and F. G. WIHSMANN, *Silikattechnik* **36** (2) (1985) 49.
17. W. BAUKAL, *Electrochim. Acta* **14** (1969) 1071.
18. B. HUDSON and P. T. MOSELEY, *J. Solid State Chem.* **19** (1976) 383.

Received 16 November 1993
and accepted 16 June 1994